

1 Dear editor,

2

3 We have revised our manuscript according to the editor's suggestions.

4

5 Best regards,

6

7 Chunsheng Zhao

8

9 **Impact of aerosol hygroscopic growth on retrieving aerosol extinction coefficient**
10 **profiles from elastic-backscatter lidar signals**

11 Gang Zhao¹, Chunsheng Zhao¹, Ye Kuang¹, Jiangchuan Tao¹, Wangshu Tan¹, Yuxuan Bian², Jing Li¹,
12 Chengcai Li¹

13 1 Department of Atmospheric and Oceanic Sciences, School of Physics, Peking University, Beijing,
14 China

15 2 State Key Laboratory of Severe Weather, Chinese Academy of Meteorological Sciences, Beijing,
16 100081, China

17 *Correspondence to: Chunsheng Zhao (zcs@pku.edu.cn)*

18 **Abstract**

19 Light detection and ranging (lidar) measurements have been widely used to profile ambient
20 aerosol extinction coefficient (σ_{ext}). ~~The Particle-particle~~ extinction-to-backscatter ratio (lidar ratio,
21 LR), which ~~highly-strongly~~ depends on ~~the~~ aerosol dry particle number size distribution (PNSD) and
22 aerosol hygroscopicity, is introduced to retrieve the σ_{ext} profile from elastic-backscatter lidar signals.
23 Conventionally, a constant column-integrated LR that is estimated from aerosol optical depth is used
24 by the retrieving algorithms. In this paper, the influences of aerosol PNSD, aerosol hygroscopic growth
25 and relative humidity (RH) profiles on the variation of LR are investigated based on the datasets from
26 field measurements in the North China Plain (NCP). Results show that LR has an enhancement factor
27 of 2.2 when RH reaches 92%. Simulation results indicate that both the magnitude and vertical
28 structures of the σ_{ext} profiles by using column-related LR method are significantly biased from the
29 original σ_{ext} profile. The relative bias, which is mainly influenced by RH and PNSD, can reach up to 40%
30 when RH at the top of the mixed layer is above 90%. A new algorithm for retrieving σ_{ext} profiles and a
31 new scheme of LR enhancement factor by RH in the NCP are proposed in this study. The relative bias
32 between the σ_{ext} profile retrieved with this new algorithm and the ideal true value is reduced to below
33 13%.

34 **1. Introduction**

35 Atmospheric aerosols can directly scatter and absorb solar radiation, thus exerting significant
36 impacts on the atmospheric environment and climate change. Vertical distributions of aerosol particles
37 are crucial for studying the roles of atmospheric aerosols in the radiation balance of the

38 Earth-Atmosphere system (Kuang et al., 2016), air pollution transportation (Gasteiger et al., 2017) and
39 boundary layer process. However, there remain many problems while determining the spatial and
40 temporal distributions of aerosols because of their highly variable properties (Anderson and Anderson,
41 2003; Andreae and Crutzen, 1997) and complex sources. As a result, our knowledge about the vertical
42 distributions of aerosols is still very limited.

43 Light detection and ranging (lidar) instruments are useful remote sensing tools to monitor profiles
44 of aerosol optical properties. This kind of instrument involves a pulsed laser beam, which can be used
45 to detect the back-scatter signals from aerosols and air molecules in the atmosphere (Klett, 1981).
46 Elastic-backscatter lidar is one of the most frequently used instruments (He et al., 2006; Pietruczuk and
47 Podgórski, 2009). However, there are some limitations when deriving aerosol extinction coefficient
48 (σ_{ext}) and aerosol back-scattering coefficient (β_{sca}) from elastic-backscatter lidar signals. Many efforts
49 have been carried out to retrieve the σ_{ext} profiles from lidar signals (Klett, 1981, 1985). Particle
50 extinction-to-backscatter ratio, which is usually termed as the lidar ratio (LR), is required when
51 retrieving σ_{ext} profiles (Fernald, 1984; Fernald et al., 1972). LR can be derived directly using Raman
52 lidar (Pappalardo et al., 2004b) and high spectral resolution lidar (She et al., 1992; Shipley et al., 1983;
53 Sroga et al., 1983) measurements. Raman lidar has low signal to noise ratios (SNR) during the day,
54 which may lead to significant bias and uncertainties in retrieving lidar signals. High spectral resolution
55 lidar have high technique requirement and expensive cost. Ansmann et al. (2002) demonstrated that the
56 profile of LR could be retrieved from Raman lidar and this LR profile can be used to retrieve σ_{ext}
57 profiles from high SNR elastic-backscattering lidar data. However, there exist many cases when
58 elastic-backscatter lidar is used without concurrently measured LR profile.

59 Sun-photometer, radiometer and elastic-backscatter lidar data are usually used simultaneously to
60 retrieve σ_{ext} profiles (Chaikovsky et al., 2016; He et al., 2006). In these studies, σ_{ext} profiles could be
61 retrieved from elastic-backscatter lidar signals by using a constant column-related LR, which is
62 constrained by measurements of aerosol optical depth (AOD) from sun-photometer. However, many
63 factors such as aerosol particle number size distribution (PNSD), aerosol refractive index, aerosol
64 hygroscopicity and ambient relative humidity (RH), have large influences on LR. It is found that the
65 ratio of σ_{ext} and β_{sca} grows linearly but slowly as RH increases when RH is lower than 80%
66 (Ackermann, 1998; Anderson et al., 2000; Ferrare et al., 2001). Further research found that LR is
67 likely to change significantly due to the substantial variation of RH in the mixed layer (Ferrare et al.,

1998). Small errors from the initial conditions may lead to large bias of retrieved σ_{ext} profiles (Sušnik et al., 2014). It is likely that using a constant LR profile instead of variable LR profile to retrieve elastic-backscatter lidar data may result in significant bias of retrieved σ_{ext} profiles. The sounding profiles show that RH is highly variable, ~~and~~ frequently ~~exceeding beyond~~ 80% in the mixed layer in the NCP (Kuang et al., 2016) which is one of the most polluted areas around the world (Ma et al., 2011; Xu et al., 2011). Accordingly ~~to this~~, it is interesting to ~~by~~ know how much σ_{ext} profiles retrieved from elastic-backscatter lidar signals will ~~deviate if a~~ ~~be deviated if~~ constant column-related LR profile is used in the NCP. Few ~~works have been done~~ ~~studies have been performed~~ to assess the bias of using a constant LR profile. This work comprehensively ~~studied~~ ~~studies~~ the possible bias by employing a large datasets of ~~the~~ field measurements.

To account for ~~the~~ aerosol hygroscopic growth, ~~the~~ κ -Köhler theory (Petters and Kreidenweis, 2007) is widely used, in which the chemical composition-~~dependent~~ variables are merged into a single parameter κ . The κ -Köhler equation is expressed as

$$\frac{RH}{100} = \frac{GF^3 - 1}{GF^3 - (1 - \kappa)} \cdot \exp\left(\frac{4\sigma_s/aM_{\text{water}}}{R \cdot T \cdot D_d \cdot g f \cdot \rho_w}\right), \quad (1)$$

where D_d is the aerosol dry diameter, GF is the aerosol growth factor, which is defined as the ratio of the aerosol diameter under the given RH and dry conditions (D_{RH}/D_d), T is the temperature, σ_s/a is the surface tension of the solution, M_{water} is the molecular weight of water, R is the universal gas constant and ρ_w is the density of water.

This article is structured in the following way. Section 2 shows all of the data used in this study. Section 3 gives the methodology of this research. Mie theory (Bohren and Huffman, 2007) and κ -Köhler theory (Petters and Kreidenweis, 2007) are used to study the influences of aerosol hygroscopic growth on LR. By calculating the LR at different RH, it is found that the RH-~~related~~ LR profiles are significantly different from the constant LR profile as shown in fig. 1(b). We simulate the bias of the retrieved σ_{ext} profiles by using the AOD related constant LR profiles in three steps. Firstly, the vertical distributions of the aerosol are parameterized and the corresponding aerosol σ_{ext} and β_{sca} profiles are calculated in section 3.2. Secondly, we calculate the theoretical signals received by the elastic-backscatter lidar in section 3.3 by using the σ_{ext} and β_{sca} profiles of the first step. Finally, we retrieve the σ_{ext} profiles from the lidar signals of section 3.3 by using the column related lidar ratio profiles, in which the method is detailed in section 3.4.1. The retrieved σ_{ext} profiles are compared with

97 | the parameterized σ_{ext} profiles. In section 3.4.2, we proposed a new method of retrieving the σ_{ext}
98 | profiles, which can account for the variations of LR with RH. Results and discussions are shown in
99 | section 4. Section 4.2 shows the bias of retrieved σ_{ext} profiles by using a column-related LR profile
100 | method. Section 4.2.1 gives the possible bias of the retrieved σ_{ext} profiles and section 4.2.2 shows the
101 | sensitivity of the bias under different AOD, different aerosol PNSD, different RH profiles and different
102 | aerosol hygroscopicity conditions. In section 4.4, ~~the~~ real-time field measurements from results of
103 | micro-pulsed lidar (MPL) are used to validate the feasibility of our new proposed method. The
104 | conclusions of this research ~~come to the~~ are summarized in section 5.

105 | 2. Data

106 | 2.1 Datasets of aerosol properties

107 | During the periods of Haze in China (HaChi) campaign, the physical and chemical properties of
108 | aerosol particles ~~are were~~ measured at the Wuqing meteorological station (39° 23' N, 117° 0' E, 7.4
109 | m a.s.l.). ~~Wuqing site~~ is located between two megacities (Beijing and Tianjin) of NCP, and can
110 | represent the pollution conditions of the NCP (Xu et al., 2011).

111 | This study uses the measured datasets of PNSD, black carbon (BC) mass concentrations (Ma et al.,
112 | 2012) and aerosol hygroscopicity (Chen et al., 2014; Liu et al., 2014) during the field campaign. The
113 | sampled aerosols particles are selected to have an aerodynamic diameter of less than 10 μm by an
114 | impactor at the initial inlet. These particles are carefully dried to below 40% RH and then led to the
115 | corresponding instruments. The aerosol PNSDs with particle diameter in the range from 10nm to 10 μm
116 | are measured by jointly using a differential mobility particle sizer (TDMPS, Leibniz Institute for
117 | Tropospheric Research, Germany; Birmili et al., 1999) and an aerodynamic particle sizer (APS, TSI
118 | Inc., model 3321) with a temporal resolution of 5 min. The BC mass concentrations are measured by a
119 | multi-angle absorption photometer (MAAP model 5012, Thermo, Inc., Waltham, MA USA). The
120 | aerosol hygroscopicity is measured by using the humidity tandem differential mobility analyzer
121 | (HTDMA), which measures the aerosol GF as a function of RH at different diameter. The aerosol
122 | hygroscopicity parameter κ can be directly derived from measurements of the HTDMA by applying
123 | formula (1).

124 | 2.2 RH profiles

125 | The intensive GTS1 observation (Bian et al., 2011) at the meteorological bureau of Beijing (39°48'

126 N,116° 28' E) were carried out from July to September, ~~in~~ 2008. With a resolution of 10m in the
127 vertical direction, the radiosonde data includes profiles of temperature, pressure and RH. During the
128 intensive observation period, balloon soundings were performed four times a day.

129 Water vapor mixing ratio is almost constant in the mixed layer due to extensive turbulent mixing,
130 ~~existing~~ and decreases rapidly above the mixed layer. RH profiles that exhibit well-mixed vertical
131 structures are ~~picked-out~~ were selected and studied. ~~With this, the maximum RH in the vertical~~
132 ~~direction can be used as a good representation of RH profiles.~~ RH profiles are classified into four
133 typical groups based on the maximum RH ranges: 60%-70%, 70%-80%, 80%-90% and 90%-95%
134 (Kuang et al., 2016). These four kinds of typical well-mixed RH profiles are labeled as P60-70, P70-80,
135 P80-90 and P90-95 respectively. These four kinds of RH profiles, which are shown in fig. 1(a), are
136 used to conduct the sensitivity studies in this article.

137 **2.3 MPL signals**

138 A single wavelength polarization diversity elastic lidar system is installed on the roof of the
139 physics building in Peking University. This instrument is a MPL manufactured by Sigma Space, using
140 a Nd: YVO4 532nm pulsed DC10H-532SS laser source, with a pulse duration of 10.3ns, energy of
141 6-8uJ and a repetition of 2500Hz. It collects elastically backscattered signals from the atmosphere by
142 separately detecting its parallel and cross polarization components with respect to the polarization of
143 laser. We also used the concurrently measured AOD data from the AERONET BEIJING_PKU station,
144 which is located at the same place as the Lidar.

145 **3. Methodology**

146 **3.1 Influences of aerosol hygroscopic growth on LR**

147 **3.1.1 Calculate the LR values under different RH conditions**

148 In this ~~research~~ paper, the Mie model (Bohren and Huffman, 2007) is used to study the influence of
149 RH on LR. When running the Mie model, aerosol PNSD, aerosol complex refractive index, black
150 carbon mixing state and black carbon mass concentrations are essential. The results of the Mie model
151 contain the information ~~of the~~ about σ_{ext} and β_{sca} , which can be used to calculate the LR directly,
152 with $\text{LR} = \frac{\sigma_{\text{ext}}}{\beta_{\text{sca}}}$.

153 When exposed to ~~the ambient water content~~, the aerosols ~~grow~~ get ~~hygroscopic~~ growth. To
154 account for this, we use the size-resolved hygroscopicity parameter κ , which is derived from the

155 measurements of the HTDMA (Chen et al., 2012; Liu et al., 2011), ~~is used in this study. The used~~ This
156 size-resolved κ is shown in fig. S1. Mean ~~value distribution~~ of the size-resolved κ during the Hachi
157 Campaign is used. With this, the aerosol GF ~~of for~~ different ~~size at different~~ D_p and RH can be
158 calculated by applying formula (1).

159 Mixing states of BC come from the measurements s during the Hachi Campaign. In previous work,
160 BC mixing states during the Hachi campaign were presented as both core-shell mixed and externally
161 mixed (Ma et al., 2012). Ma et al. (2012) provides the ratio of BC mass concentration under externally
162 mixed state, M_{ext_BC} , to total BC mass concentration, M_{BC} , as follows:

$$163 \quad r_{ext_BC} = \frac{M_{ext_BC}}{M_{BC}} \quad (2).$$

164 ~~M_{ext_BC} is the mass concentration that is externally mixed and M_{BC} is the total mass concentration of~~
165 ~~BC.~~ The mean value of $r_{ext_BC}=0.51$ (Ma et al., 2012) is used as a representation of the mixing state in
166 this study. The size-resolved distribution of BC mass concentration is the same as that used by Ma et al
167 (2012a).

168 The refractive index (\tilde{m}), ~~with~~ accounting for the water content in the particle, is derived as a
169 volume mixture between the dry aerosol and water (Wex et al., 2002):

$$170 \quad \tilde{m} = f_{V,dry} \tilde{m}_{aero,dry} + (1 - f_{V,dry}) \tilde{m}_{water} \quad (3).$$

171 $f_{V,dry}$ is the ratio of the dry aerosol volume to total aerosol volume at given RH condition; $\tilde{m}_{aero,dry}$ is
172 the refractive index of dry ambient aerosols and \tilde{m}_{water} is the refractive index of water ~~content~~
173 ~~absorbed by aerosols~~. The refractive indices of BC, non-light-absorbing aerosols and water, which are
174 used in this study, are $1.8+0.54i$ (Kuang et al., 2015), $1.53+10^{-7}i$ (Wex et al., 2002) and $1.33+10^{-7}$
175 respectively.

176 To sum up, we can calculate the LR of a PNSD under the given RH condition by using the Mie
177 scattering model. For a dry aerosol PNSD, the corresponding aerosol PNSD at a given RH can be
178 calculated by applying the mean distribution of size resolved κ and formula (1). Aerosol refractive
179 index can be determined from formula (3), too. With this information, LR can be calculated. For each
180 aerosol PNSD, we change the RH from 40% to 95% to calculate the LR values at different RH. Finally,
181 the LR values of different measured aerosol PNSD at different RH are calculated by using the same
182 method.

183 **3.1.2 Parameterizing the variation of LR with RH**

184 When the LR values under different RH are statistically studied, we find that the LR can be
185 enhanced when the RH increases, which will be discussed in detail in section 4.1.1 and fig 2.

186 The LR enhancement factor is introduced to describe the influence of aerosol hygroscopic growth
187 on LR at different RH. It is defined as the ratio of LR at a given RH to LR at the condition of RH<40%.
188 We give the statistically mean relationships between the LR enhancement factor and RH. The LR
189 enhancement factor can account for the ~~incensement-increase~~ of LR with RH and the parameterized
190 LR enhancement factor is further used in our proposed method to retrieve the σ_{ext} profiles.

191 3.2 LR profiles and σ_{ext} profiles

192 ~~Assumptions about aerosol properties in the vertical direction are made to calculate LR profiles~~
193 ~~and σ_{ext} profiles.~~

194 Liu et al. (2009) studied vertical profiles of aerosol total number concentration (Na) with aircraft
195 measurements, ~~and derived a parameterized vertical distribution. In this scheme, .—Vertical~~
196 ~~distributions of Na are parameterized according to the vertical distribution properties of Na. Results~~
197 ~~showed that~~ Na is relatively constant in the mixed layer. ~~A, with a~~ transition layer where ~~Na it~~ linearly
198 decreases ~~and an-exists in the parameterized scheme. Na also~~ exponentially decreases ~~of Na~~ above the
199 transition layer. The same parameterized scheme proposed by Liu et al. (2009) is adopted by this study.
200 Both the study of Liu et al. (2009) and Ferrero et al. (2010) manifests that the dry aerosol PNSD in the
201 mixed layer varies little. The shape of ~~the~~ dry aerosol PNSD is assumed constant ~~along~~ with ~~the~~ height,
202 which means that aerosol PNSD at different heights divided by Na give the same normalized PNSD.

203 As for the BC vertical distribution, Ferrero et al. (2011) and Ran et al. (2016) demonstrate that BC
204 mass concentration in the mixed layer remains relatively constant and decreases sharply above the
205 mixed layer. According to this, ~~the~~ parameterization scheme of BC vertical distributions ~~s~~ is assumed ~~to~~
206 ~~be~~ the same as that of ~~the~~ aerosol. The shape of the size-resolved BC mass concentration distribution is
207 also assumed ~~to be~~ the same as that at the surface.

208 LR profiles and σ_{ext} profiles can be calculated by Mie theory under these assumptions. Details of
209 computing σ_{ext} profiles can be found at Kuang et al. (2015). The calculated LR profiles and σ_{ext}
210 profiles are used in the following study to provide the theoretical elastic-backscatter signals.

211 3.3 Simulated elastic-backscatter lidar signals

212 The intensity of signals received by elastic-backscatter lidar depends on optical properties of
213 objects and the distance between scattering objects and receiving system. It can be typically described

214 by the following formula:

$$215 \quad P(R) = C \times P_0 \times \frac{\beta(R)}{R^2} \times e^{\int_0^R -2 \times \sigma(r) \times dr} \quad (4).$$

216 In formula (4), P_0 is the intensity of the laser pulse, R is the spatial distance between scattering
217 objects and the receiving system, C is a correction factor determined by the status of
218 elastic-backscatter lidar machine itself, $\beta(R)$ refers to the sum of aerosol backscattering coefficient
219 (β_{sca}) and air molecule backscattering coefficient ($\beta_{\text{sca,mole}}$) at distance R , $\sigma(R)$ denotes the sum of σ_{ext}
220 and air molecule's extinction coefficient ($\sigma_{\text{ext,mole}}$). $\beta_{\text{sca,mole}}$ and $\sigma_{\text{ext,mole}}$ can be calculated by using
221 Rayleigh scattering theory when the temperature and pressure are available.

222 In this study, we can theoretically get the intensities of elastic-backscatter lidar signals and the
223 AOD from each given σ_{ext} and β_{sca} profiles with the assumption that C is equal to one. Retrieving
224 elastic-backscatter lidar signals can result in exactly the same σ_{ext} profile as the original one when the
225 profile of LR is available. However, using a constant column-related LR profile ~~is used~~ to retrieve
226 elastic-backscatter lidar signals and will cause the retrieved σ_{ext} profile ~~would~~ deviate from the given
227 initial σ_{ext} profile ~~when there is insufficient information about the LR profile~~.

228 **3.4 Retrieving σ_{ext} profiles from elastic-backscatter lidar signals**

229 **3.4.1 Retrieving σ_{ext} profiles by using constant column-related LR profile method**

230 Traditionally, the AOD from sun-photometer and the elastic-backscatter lidar signals are
231 combined to retrieve the σ_{ext} profiles. Additional information is needed to get the mathematical results
232 of formula (4) because there are two unknown parameters (β_{sca} and σ_{ext}). The commonly used method
233 of solving this formula is to assume a constant value of column-related LR and then the profiles of σ_{ext}
234 and β_{ext} can be retrieved (Fernald, 1984; Klett, 1985). Different values of column-related LR can lead
235 to different σ_{ext} profiles and different AOD. A constant column-related LR can be constrained if the
236 sun photometer is concurrently measuring the AOD (He et al., 2006; Pietruczuk and Podgorski, 2009).
237 Thus, the σ_{ext} profile can be retrieved by using the column-related constant LR profile.

238 **3.4.2 Retrieving σ_{ext} profiles accounting for aerosol hygroscopic growth**

239 A new method of retrieving σ_{ext} profiles from elastic-backscatter lidar signals is proposed, in
240 which the variation of LR with RH can be taken into consideration. This new method requires the
241 measured elastic-backscatter lidar signals, measured AOD data and RH profiles.

242 A schematic diagram of this method is shown in Fig.2. A parameterized LR profile is used to

243 retrieve σ_{ext} profiles instead of an AOD-constrained constant LR profile. Firstly, the LR enhancement
244 factors are statistically studied and parameterized under different polluted conditions. The results of
245 ~~the~~ mean parameterized LR enhancement factor, which is detailed in section 4.1.1, are used in this
246 study. ~~The~~ LR profile can be calculated by using ~~the~~ RH profile, a LR ~~for dry aerosol value at dry state~~
247 and the equations of LR enhancement factor. ~~The~~ σ_{ext} profile can be retrieved with ~~a~~ combination of
248 LR profile and formula (4). ~~The~~ ~~d~~ Dry state LR value can be constrained by comparing the integrated
249 AOD value ~~of the~~ retrieved σ_{ext} profile and concurrently measured AOD value. ~~The~~ LR profile is
250 determined and ~~the~~ σ_{ext} profile can be retrieved with the constrained dry state LR.

251 4. Results and Discussion

252 4.1 LR properties

253 4.1.1 Variation of LR with RH

254 During the field campaign of Hachi, ~~there is a total~~ 3540 different aerosol PNSDs ~~were measured~~.
255 These aerosol PNSDs can be used as a good ~~representation~~ ~~representative~~ datasets ~~of for~~ the
256 continental aerosol. LR is calculated by using different aerosol PNSD and RH values between 30%
257 and 95%.

258 Relationships between ~~the~~ dry state LR and concurrently measured σ_{ext} (sum of the aerosol
259 scattering and absorption) are shown in Fig. 2(a). It shows that LR can vary across a wide range from
260 30 sr to 90 sr, which is consistent with the literature values of continental aerosols (Ansmann et al.,
261 2001; Pappalardo et al., 2004a). This also indicates that calculating the LR by using Mie theory is
262 feasible. Fig. 2(b) gives the probability distribution function of the LR. Most of the LR lies in the
263 range between 45~65 sr.

264 By calculating the LR values under different RH, we find that the LR tends to increase with RH.
265 Relationships between the LR enhancement factor and RH are given in Fig. 2(c). The LR enhancement
266 factor has a mean value lower than 1.2 when the RH is lower than 70%. LR increases linearly with RH
267 when RH is lower than 80%, ~~which is consistent with the literal results (Salemink et al., 1984)~~.
268 However, LR can be enhanced by a factor of 2.2 when the RH reaches 92% with mean hygroscopicity
269 of aerosol.

270 Mean values of LR enhancement factor are parameterized as below:

$$271 \quad RH_0 = RH - 40 \quad (5)$$

272
$$LR = LR_{dry} \times (0.92 + 2.5 \times 10^{-2}RH_0 - 1.3 \times 10^{-4}RH_0^2 + 2.2 \times 10^{-5}RH_0^3) \quad (6).$$

273 This parameterization equation can be used as a representation of the mean effect of continental
274 aerosol hygroscopicity on LR.

275 The ~~increase~~~~incensement~~ of LR with RH has been studied before. Ackermann (1998) calculated ~~ds~~
276 the relationships of LR with RH by using the lognormal distribution of aerosols as the input of Mie
277 scattering theory and finds that the LR increases with RH for ~~the~~ continental aerosols. However,
278 Ackermann (1998) shows that the LR doesn't show the same properties for maritime aerosols and
279 desert aerosols.

280 We theoretically analyze the reasons for the behavior of ~~the~~ LR by using the Mie scattering model
281 and the mean aerosol PNSD of the Hachi campaign. By definition, LR is the ratio of σ_{ext} to β_{sca} . β_{sca} can
282 be written as $\beta_{sca} = \frac{\sigma_{ext} \times SSA \times PF(180)}{4 \times \pi}$, where the SSA is single scattering albedo, which is defined as
283 the ratio of extinction coefficient and scattering coefficient. PF(180) is the aerosol scattering phase
284 function at the scattering angle of 180° . Thus, $LR = \frac{\sigma_{ext} \times 4 \times \pi}{\sigma_{ext} \times SSA \times PF(180)} = \frac{4 \times \pi}{SSA \times PF(180)}$. We use the mean
285 aerosol PNSD as the input of Mie scattering model and calculate the aerosol phase function and SSA
286 values at different RH. When particle grows, there tends to be larger partition of forward scattering and
287 PF(180) is smaller, which is shown in fig.S2. The PF(180) decreases by 40% from 0.27 to 0.16. At the
288 same time, the SSA increases 5% from 0.93 to 0.97 and PF(180) as shown in fig.S3. Thus, the LR
289 increases with the ~~incensement~~increase of RH.

290 4.1.2 LR ratio profiles

291 Four different types of RH profiles and LR profiles are shown in fig 1. In Fig. 1(a), RH values
292 increase with height in the mixed layer and decrease with height above the mixed layer. This is a
293 synthetic result of temperature and water content distributions in the vertical direction. In the summer
294 afternoon, water vapor is well mixed within the mixed layer and decreases sharply above ~~the mixed~~
295 layer. P60-70 can represent the relatively dry environmental conditions. Statistical results show that
296 P80-90 is most likely to be observed in the environment. P90-95 is a very moist environment condition
297 and its frequency of being observed is second to that of the P80-90 type.

298 Profiles of LR corresponding to RH profiles of the left column are shown in Fig. 1(b). For each
299 type of LR profile, LR increases with height in the mixed layer due to the increase of RH. At the
300 ground, the mean values of LR for each RH profiles are 38.19, 38.28, 39.53 and 40.33 sr, with a

301 standard deviation of 6.20, 6.22, 6.42 and 6.45 respectively. LR changes little from 38 sr at the ground
302 to 42 sr at the top of the mixed layer when the ambient RH is low for the RH profile of P60-70.
303 However, LR grows with a mean value from 40 sr to 60 sr with a relative difference of 50% when the
304 RH is high for the RH profile of P90-95. With such high variation of LR with RH, the retrieved σ_{ext}
305 profiles might be ~~greatly deviated~~very different when using a constant LR profile instead of a variable
306 one.

307 The black dotted line in Fig. 1(b) is one of the constant column-related LR profiles that are used as
308 an input ~~of to retrieving~~retrieve σ_{ext} profiles related to the RH profile P70-80. The constant LR has a
309 higher value at the ground and a lower value at the top of the mixed layer when compared with the
310 calculated variable LR profiles.

311 During the Hachi Campaign, LR values that are calculated by using Mie theory can change from
312 30 to 55 sr within 12 hours at the ground (about 87% of initial value). With high variation of LR over
313 time, the LR profile should be updated in time to get an accurately retrieved σ_{ext} profile. Using only
314 one measurement of LR profile to retrieve the σ_{ext} profiles may lead to great bias of retrieved results
315 (Rosati et al., 2016).

316 **4.2 Bias of retrieved σ_{ext} profiles**

317 With the parameterized σ_{ext} profiles by using the method of section 3.2, we can theoretically get
318 the AOD and the elastic-backscatter lidar signals. Then the AOD and the elastic-backscatter lidar
319 signals can be used to constrain a column-related constant LR profile and to retrieve σ_{ext} profiles.
320 Finally, the retrieved σ_{ext} profiles are compared with the parameterized σ_{ext} profiles and the differences
321 are statistically studied.

322 **4.2.1 Retrieved σ_{ext} profiles vs. original σ_{ext} profiles**

323 Fig. 4 provides an example of the retrieved σ_{ext} profile by using the variable LR profile method
324 and that by using the constant LR profile method from simulated lidar signals. These two kinds of
325 profiles can also be described as a given parameterized σ_{ext} profile and a retrieved σ_{ext} profile from
326 constant LR profile. In Fig. 4(a), the retrieved σ_{ext} profile by using a variable LR profile method is
327 demonstrated by solid line. ~~The Dotted-dotted~~ line shows the retrieved σ_{ext} profile by using a constant
328 column related LR method. Fig. 4(b) shows the relative bias of the two retrieved σ_{ext} profiles at each
329 height. Fig. 4(c) and (d) are almost the same as Fig. 4(a) and (b) respectively, except that the results of
330 Fig. 4(a) and (b) come from the RH profile of P70-80 while those of Fig. 4(c) and (d) come from the

331 RH profile of P90-95.

332 It is shown in Fig. 4(a) that the retrieved σ_{ext} by using a variable LR profile method increases with
333 height at a rate of $92.25 \text{ (Mm}^{-1}\text{km}^{-1}\text{)}$ in the mixed layer, which is consistent with the aerosol loading
334 and RH distribution. However, the retrieved σ_{ext} profile by using a constant LR profile method behaves
335 differently and decreases at a rate of $-152.87 \text{ (Mm}^{-1}\text{km}^{-1}\text{)}$. The structure of σ_{ext} profiles is different by
336 using two different methods. Moreover, the retrieved σ_{ext} from RH profile of P90-95 at the top of the
337 mixed layer is significantly deviated with a relative bias of 40%.

338 Both Fig. 4(a) and (c) show that the retrieved σ_{ext} is overestimated at the ground and
339 underestimated at the top of the mixed layer. From Fig 3(b), it can be concluded that the
340 AOD-constrained constant LR is larger than the calculated true LR at the ground and smaller at the top
341 of the mixed layer. According to formula (3), signals of the elastic-backscatter lidar received at any
342 height are proportional to the backscattering capability of the aerosols. When LR is larger, a larger
343 fraction of the signals transfer forward and less is scattered back. In order to receive the same amount
344 of signal, the backscattering coefficient should be larger and this can lead to the result of a larger σ_{ext} at
345 that layer. Thus, the σ_{ext} tends to be biased higher than the given parameterized σ_{ext} when the LR is
346 larger, and vice versa. Overall, the profiles retrieved by using an AOD-constrained LR can lead to a
347 positive bias at the ground and a negative bias at the top of mixed layer.

348 **4.2.2 Sensitivity Study**

349 Simulations are conducted to study the characteristics of the retrieved σ_{ext} profile bias between
350 using the constant column-related LR profile and variable LR profile. Different kinds of aerosol PNSD,
351 AOD, aerosol hygroscopicity and RH profiles are used. Aerosol PNSD data comes from the Hachi
352 Campaign field measurement. The sensitivity of the bias in aerosol hygroscopicity is evaluated by
353 changing the size-resolved κ value. Aerosols are defined to have high hygroscopicity when the aerosol
354 size-resolved κ value is one standard deviation above the mean of the size-resolved κ value. They are
355 defined as low hygroscopicity if the size-resolved κ value is one standard deviation below mean of the
356 size-resolved κ value. Four different kinds of RH profiles are also used in this sensitivity study. As
357 discussed in section 3.2.1, a negative bias at the top of the mixed layer is accompanied by a positive
358 bias at the ground and the largest bias happens at the top of the mixed layer. It is sufficient to focus on
359 the relative bias at the top of the mixed layer.

360 Statistical characteristics of the relative bias at the top of the mixed layer are shown in Fig. 5.

361 Different panels represent the results of different aerosol hygroscopicity. The left column shows the
362 results of low aerosol hygroscopicity. Middle panel shows results from mean aerosol hygroscopicity.
363 High aerosol hygroscopicity of particles results in the properties shown in the right panel. For each
364 panel, relationships between relative bias and AOD are shown. Different colors in each panel show the
365 results of different RH profiles. Filled colors represent the ranges of the relative bias at one standard
366 deviation of using different PNSD.

367 Every panel shows that relative bias clearly increases with the enhancement of RH in the
368 surroundings. The relative bias has a mean value of less than 10% for the RH profile of P60-70. LR
369 has little variation when the surrounding RH is low and the bias has a low value. For RH profiles of
370 P70-80 and P80-90, the relative bias increases with RH and increases strongly up to 25% when the
371 surrounding relative humidity is high. These behaviors of relative difference under difference RH
372 conditions are consistent with the change of LR with RH.

373 Filled color ranges of relative bias at given AOD and RH profile result from the variation of
374 aerosol PNSD. The LR enhancement factor can have different behavior with different aerosol PNSD
375 according to Mie scattering theory. Changing the aerosol PNSD leads to a wider range of bias when
376 the RH is higher. Fig. 5 also shows that different PNSD can change the relative bias by a mean value
377 of 10% for different polluted conditions.

378 Relative bias increases with AOD value when the AOD is low, while it remains constant when the
379 AOD is high. When AOD is low, the amount of scattered light by air molecules occupies a large
380 fraction. Air molecules have a constant LR of $\frac{8}{3}\pi$ sr according the Rayleigh scattering theory. The
381 relative bias of retrieved σ_{ext} profile is relatively small when the AOD is low. When the AOD has a
382 larger value, backscattered signals mainly depend on aerosol backscattering and the signals
383 backscattered by air molecules are negligible. Relative bias mainly reflects the impacts of aerosol
384 hygroscopicity. The mean relative bias increases from 26% to 32% at high RH conditions with the
385 increase of aerosol hygroscopicity. Aerosol hygroscopicity should be taken into account under high
386 RH conditions.

387 To sum up, RH is one of the most important factors that influence the accuracy of retrieving the
388 elastic-backscatter lidar data. Different PNSD can also lead to a large variation of relative difference.
389 The relative difference increases with the AOD when the AOD is low, but increases little when the

390 AOD is high. Under the conditions of both high values of RH and AOD, the relative bias of retrieved
391 data reaches a maximum due to the influence of aerosol hygroscopic growth.

392 **4.3 Evaluation of LR enhancement factor parameterization**

393 Simulations are carried out to test the accuracy of the new methods of retrieving the σ_{ext} profiles,
394 which is proposed in section 3.4.2. These simulations employ the elastic-backscattering lidar signals
395 from section 3.3, the RH profiles, the integrated AOD values of the parameterized σ_{ext} profiles and the
396 parameterization scheme of LR enhancement factor formulas (5), (6). With this information, the σ_{ext}
397 profiles are retrieved by the method of section 3.4.2. We then studied the relative biases between the
398 parameterized σ_{ext} profiles and the retrieved σ_{ext} profiles by using the new method.

399 Different kinds of aerosol PNSD, AOD, aerosol hygroscopicity and RH profiles are used in the
400 simulations. The relative bias are statistically studied and summarized. The values listed in Table 1 are
401 the mean relative biases under different PNSD conditions. From Table 1, we can see that all of the
402 relative bias is within the range of 13% for different PNSD, AOD, aerosol hygroscopicity and RH
403 profiles. This indicates that the algorithm of using the mean LR enhancement factor parameterization
404 scheme is feasible and can decrease the bias of the retrieved elastic-backscatter lidar data significantly.

405 **4.4 Retrieving the real-time measurement elastic-backscatter lidar signals**

406 MPL data and AERONET data are employed to validate the algorithm of retrieving the
407 elastic-backscatter lidar data on the day of 5 July 2016. After quality control of data processing,
408 elastic-backscatter lidar data is retrieved by using both a constant LR profile method and a
409 parameterized variable LR profile method. Details of retrieving the MPL signals and the auxiliary
410 information are shown in fig.S5. Fig. 6 gives the retrieved σ_{ext} profiles ~~using for two methods~~ of local
411 times 13:00 (a) and 14:30 (b).

412 Fig. 6(a) is a typical case of the retrieved σ_{ext} profiles under high values of both RH and AOD
413 conditions. The retrieved σ_{ext} profiles by using the constant LR profile method and variable LR profile
414 method show almost the same properties as the simulations. The relative bias reaches a value of 39.3%
415 at an altitude of 1.57 km. These differences of retrieved σ_{ext} profiles may lead to a significant bias of
416 estimating the mixed layer height and have significant impact on radiative energy distribution in the
417 vertical direction. Fig. 6(b) shows the retrieved σ_{ext} profiles of different structures from the same
418 elastic-backscatter lidar data. The retrieved σ_{ext} by using variable LR profile method increases with
419 height within the mixed layer. However, the retrieved σ_{ext} by using constant LR profile decreases

420 slightly with height within the mixed layer.

421 **5 Conclusions**

422 The influence of aerosol hygroscopic growth on LR is evaluated by using Mie scattering theory.
423 Datasets used as input to Mie theory model come from the Hachi Campaign field measurements and
424 these datasets can be used as a good representation of the continental aerosols. Results show that LR in
425 the NCP mainly ranges from 30 to 90 sr, which is consistent with literature values of continental
426 aerosols. LR could be enhanced significantly under high RH conditions, with a mean factor of 2.2 at
427 92% RH.

428 RH in the mixed layer in the NCP is frequently observed to be higher than 90%. Under these
429 conditions, a large variation of LR in the vertical direction exists. This leads to significant bias of
430 retrieved σ_{ext} profile due to a constant LR profile currently used to retrieve the elastic-backscatter lidar
431 signals. The relative bias of the retrieved σ_{ext} profiles between the constant LR profile method and the
432 variable LR profile method can reach up to 40% under high RH conditions ~~and the retrieved σ_{ext}~~
433 ~~profile structure can be different under low RH conditions.~~

434 Sensitivity studies ~~are~~ were carried out to test the bias of retrieved σ_{ext} profiles. The bias ~~increases~~
435 increased linearly with RH at low RH but ~~increases~~ increased strongly at high RH. Different PNSDs
436 can lead to 10% standard deviation of the bias. Maximum bias happens under the conditions of both
437 high AOD and RH that frequently happen in the NCP. The influence of aerosol hygroscopic growth on
438 LR should be taken into consideration when retrieving the elastic-backscatter lidar data in the NCP.

439 A new algorithm accounting for the aerosol hygroscopic growth is proposed to retrieve the
440 elastic-backscatter lidar data. A scheme of LR enhancement factor parameterization is introduced in
441 this algorithm. The bias of retrieved σ_{ext} profiles by using this algorithm can be constrained within
442 13%. Real-time measurement of MPL data is employed to validate the algorithm and the results show
443 good consistency with the simulations.

444 This research will advance our understanding of the influence of aerosol hygroscopic growth on
445 LR and help to improve the retrieval of σ_{ext} profile from elastic-backscatter lidar signals.

446

447 **Acknowledgments**

448 This work is supported by the National Natural Science Foundation of China (41590872,

449 41375134).

450

451

452 **References**

453 Ackermann, J. (1998) The Extinction-to-Backscatter Ratio of Tropospheric Aerosol: A Numerical Study. *Journal of*
454 *Atmospheric and Oceanic Technology* 15, 1043-1050.

455 Anderson, T.L., Anderson, T.L. (2003) Variability of aerosol optical properties derived from in situ aircraft measurements
456 during ACE-Asia. *Journal of Geophysical Research* 108, ACE-15-11-ACE 15-19.

457 Anderson, T.L., Masonis, S.J., Covert, D.S., Charlson, R.J., Rood, M.J. (2000) In situ measurement of the aerosol
458 extinction-to-backscatter ratio at a polluted continental site. *Journal of Geophysical Research: Atmospheres* 105,
459 26907-26915.

460 Andreae, M.O., Crutzen, P.J. (1997) Atmospheric Aerosols: Biogeochemical Sources and Role in Atmospheric Chemistry.
461 *Science* 276, 1052-1058.

462 Ansmann, A., Wagner, F., Althausen, D., Müller, D., Herber, A., Wandinger, U. (2001) European pollution outbreaks during
463 ACE 2: Lofted aerosol plumes observed with Raman lidar at the Portuguese coast. *Journal of Geophysical Research*
464 *Atmospheres* 106, 20725–20733.

465 Ansmann, A., Wagner, F., Müller, D., Althausen, D., Herber, A., von Hoyningen-Huene, W., Wandinger, U. (2002) European
466 pollution outbreaks during ACE 2: Optical particle properties inferred from multiwavelength lidar and star-Sun photometry.
467 *Journal of Geophysical Research: Atmospheres* 107, AAC 8-1-AAC 8-14.

468 Bian, J., Chen, H., Ouml, mel, H., Duan, Y. (2011) Intercomparison of humidity and temperature sensors: GTS1, Vaisala RS80,
469 and CFH. *Advances in atmospheric sciences* 28, 139-146.

470 Bohren, C.F., Huffman, D.R., (2007) Absorption and Scattering by an Arbitrary Particle, Absorption and Scattering of Light
471 by Small Particles. Wiley-VCH Verlag GmbH, pp. 57-81.

472 Chaikovsky, A., Dubovik, O., Holben, B., Bril, A., Goloub, P., Tanre, D., Pappalardo, G., Wandinger, U., Chaikovskaya, L.,
473 Denisov, S., Grudo, J., Lopatin, A., Karol, Y., Lapyonok, T., Amiridis, V., Ansmann, A., Apituley, A., Allados-Arboledas, L.,
474 Biniatoglou, I., Boselli, A., D'Amico, G., Freudenthaler, V., Giles, D., Jose Granados-Munoz, M., Kokkalis, P., Nicolae, D.,
475 Oshchepkov, S., Papayannis, A., Perrone, M.R., Pietruczuk, A., Rocadenbosch, F., Sicard, M., Slutsker, I., Talianu, C., De
476 Tomasi, F., Tsekeri, A., Wagner, J., Wang, X. (2016) Lidar-Radiometer Inversion Code (LIRIC) for the retrieval of vertical
477 aerosol properties from combined lidar/radiometer data: development and distribution in EARLINET. *Atmospheric*
478 *Measurement Techniques* 9, 1181-1205.

479 Chen, J., Zhao, C.S., Ma, N., Liu, P.F., Göbel, T., Hallbauer, E., Deng, Z.Z., Ran, L., Xu, W.Y., Liang, Z., Liu, H.J., Yan, P., Zhou,
480 X.J., Wiedensohler, A. (2012) A parameterization of low visibilities for hazy days in the North China Plain. *Atmos. Chem.*
481 *Phys.* 12, 4935-4950.

482 Chen, J., Zhao, C.S., Ma, N., Yan, P. (2014) Aerosol hygroscopicity parameter derived from the light scattering enhancement
483 factor measurements in the North China Plain. *Atmos. Chem. Phys.* 14, 8105-8118.

484 Fernald, F.G. (1984) Analysis of atmospheric lidar observations: some comments. *Applied Optics* 23, 652-653.

485 Fernald, F.G., Herman, B.M., Reagan, J.A. (1972) Determination of Aerosol Height Distributions by Lidar. *Journal of Applied*
486 *Meteorology* 11, 482-489.

487 Ferrare, R.A., Melfi, S.H., Whiteman, D.N., Evans, K.D., Poellot, M., Kaufman, Y.J. (1998) Raman lidar measurements of
488 aerosol extinction and backscattering: 2. Derivation of aerosol real refractive index, single-scattering albedo, and
489 humidification factor using Raman lidar and aircraft size distribution measurements. *Journal of Geophysical Research:*
490 *Atmospheres* 103, 19673-19689.

491 Ferrare, R.A., Turner, D.D., Brasseur, L.H., Feltz, W.F., Dubovik, O., Tooman, T.P. (2001) Raman lidar measurements of the
492 aerosol extinction-to-backscatter ratio over the Southern Great Plains. *Journal of Geophysical Research: Atmospheres* 106,
493 20333-20347.

494 Ferrero, L., Mocnik, G., Ferrini, B.S., Perrone, M.G., Sangiorgi, G., Bolzacchini, E. (2011) Vertical profiles of aerosol
495 absorption coefficient from micro-Aethalometer data and Mie calculation over Milan. *Science of the Total Environment*
496 409, 2824-2837.

497 Ferrero, L., Perrone, M.G., Petraccone, S., Sangiorgi, G., Ferrini, B.S., Lo Porto, C., Lazzati, Z., Cocchi, D., Bruno, F., Greco, F.,
498 Riccio, A., Bolzacchini, E. (2010) Vertically-resolved particle size distribution within and above the mixing layer over the
499 Milan metropolitan area. *Atmospheric Chemistry and Physics* 10, 3915-3932.

500 Gasteiger, J., Groß, S., Sauer, D., Haarig, M., Ansmann, A., Weinzierl, B. (2017) Particle settling and vertical mixing in the
501 Saharan Air Layer as seen from an integrated model, lidar, and in situ perspective. *Atmospheric Chemistry and Physics* 17,
502 297-311.

503 He, Q.S., Li, C.C., Mao, J.T., Lau, A.K.H., Li, P.R. (2006) A study on the aerosol extinction-to-backscatter ratio with
504 combination of micro-pulse LIDAR and MODIS over Hong Kong. *Atmospheric Chemistry and Physics* 6, 3243-3256.

505 Klett, J.D. (1981) Stable analytical inversion solution for processing lidar returns. *Applied Optics* 20, 211-220.

506 Klett, J.D. (1985) Lidar inversion with variable backscatter/extinction ratios. *Applied Optics* 24, 1638-1643.

507 Kuang, Y., Zhao, C.S., Tao, J.C., Bian, Y.X., Ma, N. (2016) Impact of aerosol hygroscopic growth on the direct aerosol
508 radiative effect in summer on North China Plain. *Atmospheric Environment* 147, 224-233.

509 Kuang, Y., Zhao, C.S., Tao, J.C., Ma, N. (2015) Diurnal variations of aerosol optical properties in the North China Plain and
510 their influences on the estimates of direct aerosol radiative effect. *Atmos. Chem. Phys.* 15, 5761-5772.

511 Liu, H.J., Zhao, C.S., Nekat, B., Ma, N., Wiedensohler, A., van Pinxteren, D., Spindler, G., Müller, K., Herrmann, H. (2014)
512 Aerosol hygroscopicity derived from size-segregated chemical composition and its parameterization in the North China
513 Plain. *Atmospheric Chemistry and Physics* 14, 2525-2539.

514 Liu, P., Zhao, C., Zhang, Q., Deng, Z., Huang, M., Xincheng, M.A., Tie, X. (2009) Aircraft study of aerosol vertical
515 distributions over Beijing and their optical properties. *Tellus Series B-Chemical & Physical Meteorology* 61, 756-767.

516 Liu, P.F., Zhao, C.S., Göbel, T., Hallbauer, E., Nowak, A., Ran, L., Xu, W.Y., Deng, Z.Z., Ma, N., Mildenerger, K., Henning, S.,
517 Stratmann, F., Wiedensohler, A. (2011) Hygroscopic properties of aerosol particles at high relative humidity and their
518 diurnal variations in the North China Plain. *Atmos. Chem. Phys.* 11, 3479-3494.

519 Ma, N., Zhao, C.S., Müller, T., Cheng, Y.F., Liu, P.F., Deng, Z.Z., Xu, W.Y., Ran, L., Nekat, B., van Pinxteren, D., Gnauk, T., Müller,
520 K., Herrmann, H., Yan, P., Zhou, X.J., Wiedensohler, A. (2012) A new method to determine the mixing state of light
521 absorbing carbonaceous using the measured aerosol optical properties and number size distributions. *Atmos. Chem. Phys.*
522 12, 2381-2397.

523 Ma, N., Zhao, C.S., Nowak, A., Müller, T., Pfeifer, S., Cheng, Y.F., Deng, Z.Z., Liu, P.F., Xu, W.Y., Ran, L., Yan, P., Göbel, T.,
524 Hallbauer, E., Mildenerger, K., Henning, S., Yu, J., Chen, L.L., Zhou, X.J., Stratmann, F., Wiedensohler, A. (2011) Aerosol
525 optical properties in the North China Plain during HaChi campaign: an in-situ optical closure study. *Atmos. Chem. Phys.* 11,
526 5959-5973.

527 Pappalardo, G., Amodeo, A., Mona, L., Pandolfi, M., Pergola, N., Cuomo, V. (2004a) Raman lidar observations of aerosol
528 emitted during the 2002 Etna eruption. *Geophysical Research Letters* 31, 179-211.

529 Pappalardo, G., Amodeo, A., Pandolfi, M., Wandinger, U., Ansmann, A., Bösenberg, J., Matthias, V., Amiridis, V., De Tomasi,
530 F., Frioud, M., Iarlori, M., Komguem, L., Papayannis, A., Rocadenbosch, F., Wang, X. (2004b) Aerosol lidar intercomparison
531 in the framework of the EARLINET project. 3. Ramanlidar algorithm for aerosol extinction, backscatter, and lidar ratio.
532 *Applied Optics* 43, 5370-5385.

533 Petters, M.D., Kreidenweis, S.M. (2007) A single parameter representation of hygroscopic growth and cloud condensation
534 nucleus activity. *Atmos. Chem. Phys.* 7, 1961-1971.

535 Pietruczuk, A., Podgórski, J., (2009) The lidar ratio derived from sun-photometer measurements at Belsk Geophysical
536 Observatory, *Acta Geophysica*, p. 476.

537 Pietruczuk, A., Podgorski, J. (2009) The lidar ratio derived from sun-photometer measurements at Belsk Geophysical
538 Observatory. *Acta Geophysica* 57, 476-493.

539 Ran, L., Deng, Z., Xu, X., Yan, P., Lin, W., Wang, Y., Tian, P., Wang, P., Pan, W., Lu, D. (2016) Vertical profiles of black carbon
540 measured by a micro-aethalometer in summer in the North China Plain. *Atmospheric Chemistry and Physics* 16,
541 10441-10454.

542 Rosati, B., Herrmann, E., Bucci, S., Fierli, F., Cairo, F., Gysel, M., Tillmann, R., Groß, J., Gobbi, G.P., Di Liberto, L.,
543 Di Donfrancesco, G., Wiedensohler, A., Weingartner, E., Virtanen, A., Mentel, T.F., Baltensperger, U. (2016) Studying the
544 vertical aerosol extinction coefficient by comparing in situ airborne data and elastic backscatter lidar. *Atmospheric
545 Chemistry and Physics* 16, 4539-4554.

546 Salemink, H.W.M., Schotanus, P., Bergwerff, J.B. (1984) Quantitative lidar at 532 nm for vertical extinction profiles and the
547 effect of relative humidity. *Applied Physics B* 34, 187-189.

548 She, C.Y., Alvarez, R.J., Caldwell, L.M., Krueger, D.A. (1992) High-spectral-resolution Rayleigh–Mie lidar measurement
549 of aerosol and atmospheric profiles. *Optics Letters* 17, 541-543.

550 Shipley, S.T., Tracy, D.H., Eloranta, E.W., Trauger, J.T., Sroga, J.T., Roesler, F.L., Weinman, J.A. (1983) High spectral resolution
551 lidar to measure optical scattering properties of atmospheric aerosols. 1: Theory and instrumentation. *Applied Optics* 22,
552 3716-3724.

553 Sroga, J.T., Eloranta, E.W., Shipley, S.T., Roesler, F.L., Tryon, P.J. (1983) High spectral resolution lidar to measure optical
554 scattering properties of atmospheric aerosols. 2: Calibration and data analysis. *Applied Optics* 22, 3725-3732.

555 Sušnik, A., Holder, H., Eichinger, W. (2014) A Minimum Variance Method for Lidar Signal Inversion. *Journal of Atmospheric
556 and Oceanic Technology* 31, 468-473.

557 Wex, H., Neususs, C., Wendisch, M., Stratmann, F., Koziar, C., Keil, A., Wiedensohler, A., Ebert, M. (2002) Particle scattering,
558 backscattering, and absorption coefficients: An in situ closure and sensitivity study. *Journal Of Geophysical
559 Research-Atmospheres* 107.

560 Xu, W.Y., Zhao, C.S., Ran, L., Deng, Z.Z., Liu, P.F., Ma, N., Lin, W.L., Xu, X.B., Yan, P., He, X., Yu, J., Liang, W.D., Chen, L.L. (2011)
561 Characteristics of pollutants and their correlation to meteorological conditions at a suburban site in the North China Plain.
562 *Atmos. Chem. Phys.* 11, 4353-4369.

563

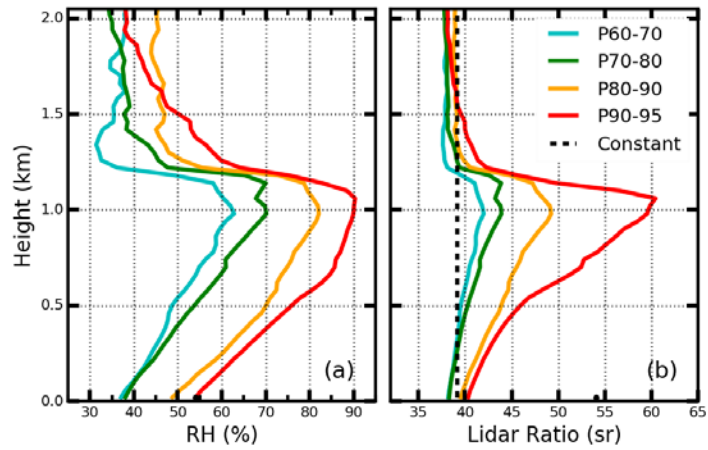
564

565 **Table 1.** Relative difference (%) between the σ_{ext} profiles by using the proposed new method and the parameterized σ_{ext}
 566 profiles under different AOD and RH profile conditions

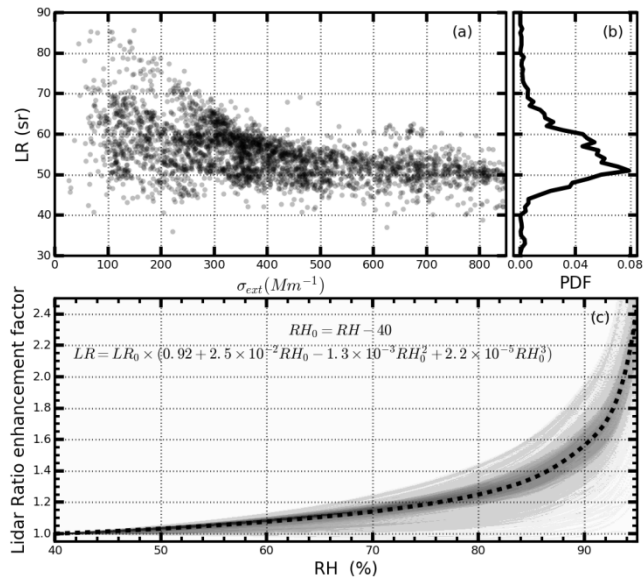
		AOD							
		0.2	0.4	0.6	0.8	1.0	1.2	1.4	1.6
RH profile	P60-70	6	9	11	13	8	8	8	9
	P70-80	7	7	9	12	7	6	7	8
	P80-90	8	5	4	11	6	5	5	6
	P90-95	9	6	6	9	13	7	7	9

567

568



569
 570 **Figure 1.** (a) Four kinds of RH profiles P60-70, P70-80, P80-90, and P90-95; (b) calculated LR profiles from the
 571 | corresponding RH profiles of (a). The Dotted black line is one of the constant LR profiles that are used to retrieve
 572 | the MPL signals.
 573



574

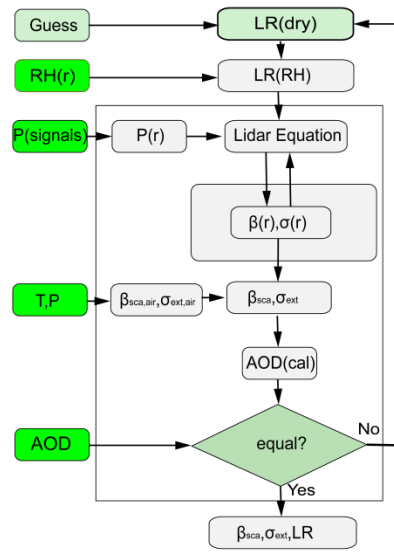
575 | **Figure 2.** LR distribution and LR enhancement factor during [the](#) Hachi campaign. (a) LR distribution under different
 576 polluted conditions. (b) Probability distribution of the LR. (c) Enhancement factor of the LR. Dotted line is the mean
 577 fit LR enhancement factor.

578

579

580

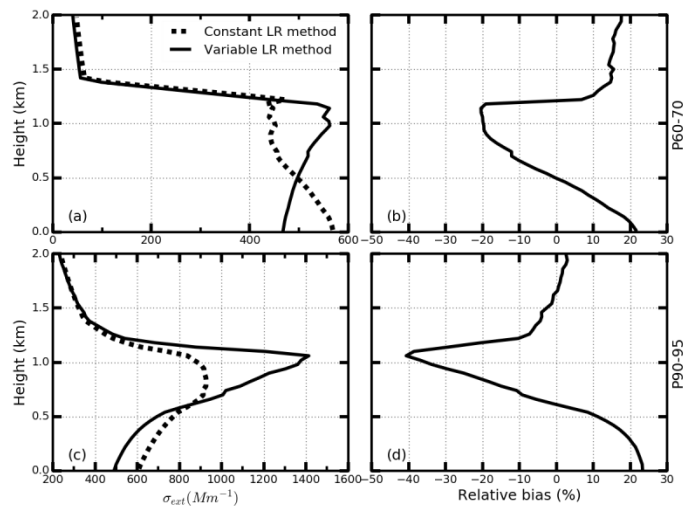
581



582

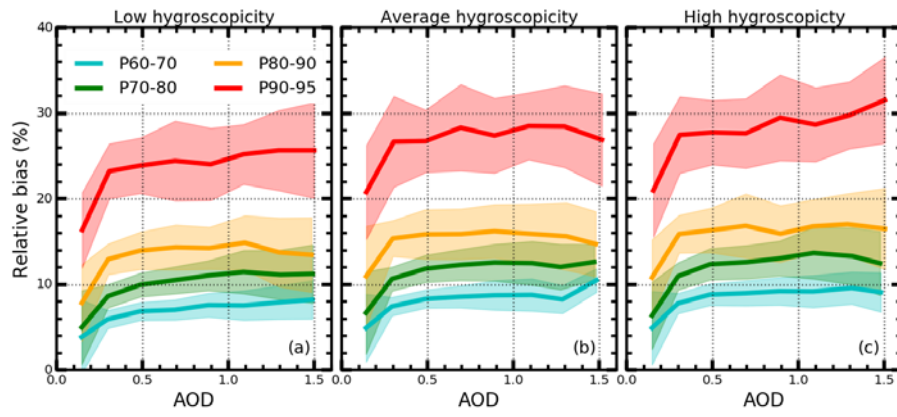
583 | **Figure 3.** Schematic diagram of retrieving the σ_{ext} profile. The input variables are displayed in a green background.

584

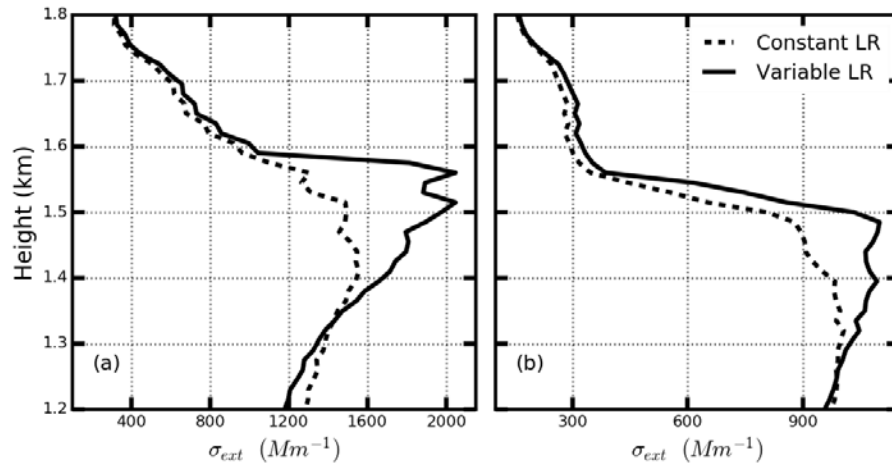


586

587 **Figure 4.** (a) Retrieved σ_{aero} profiles using constant LR profile method (dotted line) and variable LR profile method
 588 (solid line) from simulated lidar signals. (b) The relative bias of the retrieved σ_{aero} profile using two different methods.
 589 (c),(d) are the same as (a), (b) respectively. The LR signals of panel (a) results form P70-80 RH profile, and LR
 590 | signals of panel (b) results from P90-95 RH profile.



591
 592 **Figure 5.** Relative bias of the retrieved σ_{ext} under different AOD, PNSD, and hygroscopicity and RH profiles
 593 conditions. Different colors represent different RH profile. Panel (a) is derived from the low hygroscopicity. Panel (b)
 594 results from the mean hygroscopicity. Panel (c) is for high hygroscopicity.



595
 596 **Figure 6.** Retrieved σ_{ext} profiles from field measurement MPL signals at (a) 13:00 and (b) 14:30 on July 5, 2016. ~~Dotted~~
 597 The dotted line represents the retrieved σ_{ext} profiles using constant LR profile method. ~~Solid~~ The solid line represents the
 598 retrieved σ_{ext} profiles using the variable LR profile method.